JGR Oceans

RESEARCH ARTICLE
10.1029/2023JC019638

Temperature and Salinity Anomalies in the Sea Surface Microlayer of the South Pacific During Precipitation Events

L. Gassen[1], T. H. Badewien[1], J. Ewald[1,2], M. Ribas-Ribas[1], and O. Wurl[1]

[1]Center for Marine Sensors (ZfMarS), Institute for Chemistry and Biology of the Marine Environment (ICBM), Carl von Ossietzky University of Oldenburg, Wilhelmshaven, Germany, [2]German Aerospace Center (DLR), Space Agency, Bonn, Germany

Key Points:

- Small scale air-sea interactions (freshwater fluxes) during precipitation were investigated in the southern Pacific
- Temperature and salinity anomalies occur with a high spatial variability
- Measurements with remote controlled catamaran revealed shallow freshwater lenses, which were not detectable with ship based measurements

Supporting Information:

Supporting Information may be found in the online version of this article.

Correspondence to:

L. Gassen,
lisa.gassen@uni-oldenburg.de

Citation:

Gassen, L., Badewien, T. H., Ewald, J., Ribas-Ribas, M., & Wurl, O. (2023). Temperature and salinity anomalies in the sea surface microlayer of the South Pacific during precipitation events. *Journal of Geophysical Research: Oceans*, *128*, e2023JC019638. https://doi.org/10.1029/2023JC019638

Received 12 JAN 2023
Accepted 6 JUN 2023

Author Contributions:

Funding acquisition: O. Wurl
Supervision: T. H. Badewien, M. Ribas-Ribas, O. Wurl
Visualization: L. Gassen, J. Ewald
Writing – original draft: L. Gassen
Writing – review & editing: M. Ribas-Ribas, O. Wurl

© 2023. The Authors.
This is an open access article under the terms of the Creative Commons Attribution-NonCommercial-NoDerivs License, which permits use and distribution in any medium, provided the original work is properly cited, the use is non-commercial and no modifications or adaptations are made.

Abstract We present the results of salinity (ΔS) and temperature (ΔT) anomalies in the sea surface microlayer (SML) in relation to the underlying mixed bulk water (bulk). Several light to moderate rain events were recorded in the southern Pacific near Fiji using our remotely operated catamaran. Precipitation and evaporation drive freshwater fluxes across the sea surface (i.e., the SML) and are the most essential processes of the hydrologic cycle. However, measurements of the SML during precipitation are rare, but necessary to fully understand freshwater exchange at the air-sea interface. Here we show that freshwater can mix rapidly with the bulk water through wind-induced mixing, as ΔS and ΔT show a clear dependence on wind speed. At high wind speeds (5.1–11.6 m s^{-1}), anomalies approach zero ($\Delta S = -0.02 \pm 0.49$ g kg^{-1}, $\Delta T = -0.09 \pm 0.46$°C) but can reach $\Delta S = 1.00 \pm 0.20$ g kg^{-1} and $\Delta T = -0.37 \pm 0.09$°C at lower wind speeds (0–2 m s^{-1}). We find shallow freshwater lenses and fronts, likely caused by past rainfall, with ΔS and ΔT of up to −1.11 g kg^{-1} and 1.77°C, respectively. Our observations suggest that freshwater lenses can be very shallow (<1 m depth) and missed by conventional measurements. In addition, the temperature and salinity in the SML respond to freshwater fluxes instantaneously. It highlights the role of the SML in a mechanistic understanding of the fate of freshwater over the ocean and, therefore, the global hydrologic cycle.

Plain Language Summary Rain and evaporation are the most important processes in the global water cycle, causing either the supply to or the removal of freshwater from the upper ocean, thereby changing the salinity of the sea surface. Evaporation also removes heat and lowers the temperature on the ocean surface. We used the measurements of sea surface microlayer (SML) salinity and temperature as key indicators to study hydrologic cycle processes during our cruise with the RV Falkor in the South Pacific and found that freshwater mixes rapidly with the underlying bulk water during strong winds (5.1–11.6 m s^{-1}). We also detected shallow freshwater lenses and fronts, most likely caused by past rainfall, with ΔS and ΔT of up to −1.11 g kg^{-1} and 1.77°C, respectively. Our observations suggest that freshwater lenses can occur at the sea surface and that the SML respond to freshwater fluxes instantaneously. It highlights the role of the SML for future studies of the global hydrologic cycle.

1. Introduction

Precipitation and evaporation are the most essential processes of the global hydrologic cycle that cause either the supply or the removal of freshwater in the upper ocean layers, thus decreasing or increasing sea surface salinity (SSS) (Durack, 2015; Terray et al., 2012). Understanding these processes and their interplay has become increasingly important, as the hydrologic cycle is directly affected by human-induced climate change (Menon et al., 2007; Willett et al., 2007). Evaporation also has a cooling effect on sea surface temperature (SST) due to latent heat flux (Katsaros, 1980). Measurements of SSS and SST have received considerable attention due to the increasing importance of satellite observations of essential climate variables. Lindstrom et al. (2015) conducted a combined study of satellite and in situ measurements as part of the Salinity Processes in the Upper Ocean Regional Study. Rainfall events occur frequently in the tropical Pacific Ocean, inducing freshwater lenses in the upper ocean layers. Freshwater lenses can reach the size of a rain front and can accumulate more freshwater over time due to further rainfall events (Drushka et al., 2019; Moulin et al., 2021). The lifetime of the lenses can be up to 10 hr and depends mainly on wind speed (Moulin et al., 2021; Price, 1979; Thompson et al., 2019). Previous studies have described changes in salinity during precipitation events and the formation of freshwater lenses in the near-surface ocean (Asher et al., 2014; Drushka et al., 2016; Iyer & Drushka, 2021a; Katsaros & Buettner, 1969; Reverdin et al., 2020). All of these studies indicate that changes in salinity and temperature are

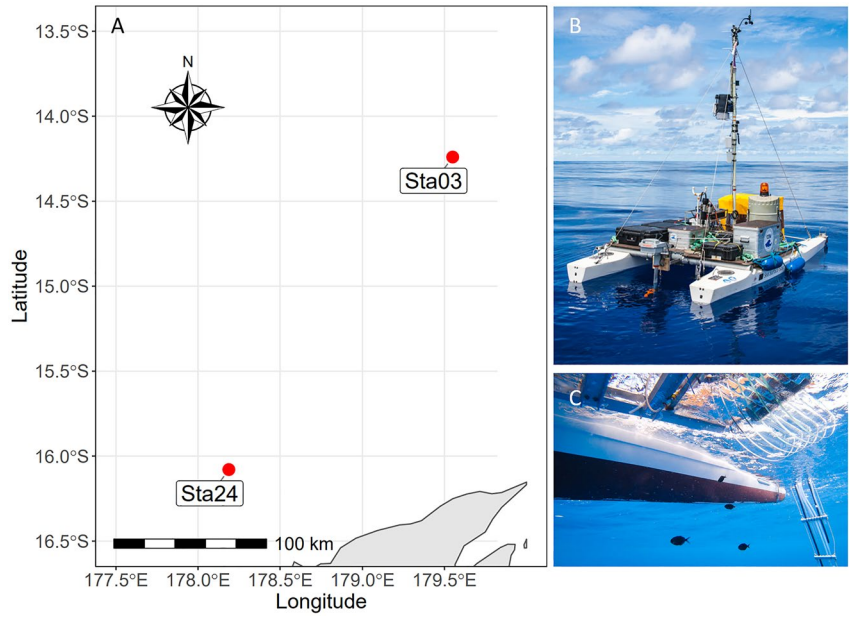

Figure 1. (a) Positions of the stations 03 (Sta03) and 24 (Sta24) in the South Pacific near Fiji islands. (b) S^3 operation with multiple sensors on board. (c) View from below of the catamaran with glass plates submerged in the water. Photo credit: Alex Ingle/Schmidt Ocean Institute.

related to rainfall rates and wind speeds. Precipitation is accompanied by changes in other atmospheric variables, such as wind speed and solar radiation (Drushka et al., 2016; Webster et al., 1996), and rainfall can suppress surface gravity waves and increase surface currents (Laxague & Zappa, 2020). Henocq et al. (2010) pointed out that there is a need for high-resolution profiles of the upper 1 m of the ocean because of its great variability. Most studies are limited to recording salinity and temperature only near the sea surface (up to 5 cm) or using satellite-derived data with daily resolutions. Measurements of SSS and SST in the SML (i.e., the upper 1,000 µm) are rare but crucial, as evaporation occurs on the surface and not in the near-surface layer, and precipitation is mixed from the surface into the near-surface layer (Wurl et al., 2019). For this reason, the relationships between precipitation and evaporation, temperature, and salinity anomalies are not fully understood.

In this study, we describe high-resolution measurements with a remote-controlled catamaran to collect the SML and the underlying bulk water during two rainfall events in the South Pacific. Our results show salinity and temperature anomalies in terms of precipitation intensity and prevailing wind speed. We describe the detection of shallow freshwater lenses and fronts, which are most likely caused by previous rainfall events. We analyzed satellite data of the SST and SSS to confirm the observed spatial variability.

2. Materials and Methods

2.1. The Study Area

The expedition FK191120 took place in the South Pacific in the geographical area of 9°–19°S, 176°E, and 175°W with the RV Falkor (20 November 2019–17 December 2019). The cruise comprised 18 stations. Precipitation occurred during the operation of our catamaran at two stations. In this paper, we focus on these two stations: 03 (23 November 2019) and 24 (15 and 16 December 2019) (Figure 1a). At Station 03, the instruments were deployed from 01:52 to 03:50 UTC and included two precipitation events with lengths of 16 and 25 min. At station 24, the deployment took place from 19:40 to 01:30 UTC and also included two rainfall events with a length of 16 and 23 min.

2.2. Capture Temperature and Salinity Anomalies With the Sea Surface Scanner (S^3)

SSS (determined from conductivity) and SST were measured with the remote-controlled catamaran Sea Surface Scanner (S^3), which is equipped with an assembly of six continuously rotating glass discs to collect the SML

of about 80 μm in thickness (Ribas-Ribas et al., 2017). Due to surface tension, the SML layer adhered to the partially immersed glass discs and was removed by scrapers positioned between the discs and pumped through in situ sensors (Figures 1b and 1c). Rotating glass discs have been shown to sample SML effectively (Shinki et al., 2012). Simultaneous measurements from infrared cameras capable of measuring skin temperatures of about 20 μm and measurements of SST from the S^3 showed comparable results (Wurl et al., 2019). S^3 was equipped with a non-transparent hood over the glass discs to reduce evaporation processes from the rotating glass discs. Still, breaking waves may occasionally splash the plates and dilute the skin layer, leading to an underestimation of the calculated temperature and salinity anomalies. However, 69% of the observed wind speeds were below 7 m s^{-1}, and less than 10% of the total number of waves break at 7 m s^{-1} (Holthuijsen & Herbers, 1986). A constant rotation speed of 7.5 per min was set for glass disc sampling. The bulk water from a depth of 1 m was sampled simultaneously. The temperature was measured with a PT1000 with an accuracy of 0.1°C (Model MU6100, VWR, Belgium). Conductivity was measured with a two-pole graphite sensor with an accuracy of 0.2% (Model MU6100, VWR, Belgium), calibrated with a standard reference material (P-Serie, IAPSO). Salinity was computed from conductivity and temperature measurements, according to Gill and Adrian (1982). Sigma-*t* is defined as the density and was calculated from the determined temperature and salinity minus 1,000 kg m^{-3}. Data collected at a frequency of 0.1 Hz were logged and averaged over each minute or over 3 min for smoothing. Meteorological variables, such as wind speed, air temperature, humidity, and rain rate, were measured 2 m above the water surface using a weather station (Vantage Pro2, Davis Instruments). The wind speed was converted to a height of 10 m (U_{10}), using the following equation (Kleemann & Meliß, 1993):

$$U_{10} = W * \left((10/H_{S^3})^g\right) \quad (1)$$

Here W is the wind speed captured by the weather station of S^3. H_{S^3} describes the height of the wind speed measurement on the S^3, which was 2 m. The exponent g depends on the environment, we chose $g = 0.16$, which is typical of oceanic conditions.

Salinity and temperature anomalies (ΔS, ΔT) were calculated as the difference between the values from the SML and bulk of 1 m depth (±0.1 m), that is, ΔS = salinity SML-salinity bulk (1-m depth) and ΔT = temperature SML-temperature bulk (1-m depth), respectively. We collected discrete water samples at each station to determine salinity from the outflow of the flow-through system. The salinity of the discrete water samples was analyzed at the GEOMAR laboratory in Kiel using a salinometer (8410A Portasal™, GUIDELINE Instruments) to validate the computed salinity of the catamaran S^3.

2.3. Ship Based Measurements and Calculation of the Evaporation Rate

The shortwave radiation data were continuously logged by the shipboard's automated meteorological and oceanographic system. Additionally, a laser precipitation monitor (THIES Clima, 5.4110.xx.x00) was installed on the RV Falkor, which captured the rain rate and the rain amount. Complementary data from a thermosalinograph (TSG) mounted on R/V Falkor provide additional observations of bulk water at nominal depth of 3 m. The TSG is equipped with a SeaBird SBE-45 sensor to measure conductivity and temperature. Evaporation rates were computed using the COARE algorithm (Fairall et al., 1996). Most of the parameters that contributed to the evaporation calculation were measured by the S^3 weather station, such as wind speed, air temperature, humidity, and rain rate. Solar radiation used for the calculation was only measured on the ship and not S^3.

2.4. Remote Sensing Images

The SSS remote sensing images were processed from the Soil Moisture and Ocean Salinity (SMOS) daily global L4 products (0.05° × 0.05°, Barcelona Expert Center), which are computed from the L3 product using the multifractal fusion technique (Olmedo et al., 2021). They are used as an indicative measure of daily SSS in this study, because L2 products did not show coverage of the operational areas (see Figure S3 in Supporting Information S1). The SSS measurements with SMOS covered the first upper centimeter of the sea surface. An hourly mean L4 operational sea surface temperature and sea ice analysis SST skin product (0.25° × 0.25°) was used to show the variability of SST in the surrounding areas of stations 03 and 24 (Donlon et al., 2007). The SST skin product represents the surface temperature at a depth of 10–20 μm and is the one closest to the SML. The SST images show the mean SST for the entire deployment time (four hourly datasets: 01:00–04:00 UTC). The SSS

and SST differences with the lowest value (SSS/SST-lowest SSS/SST) were calculated to show relative values. Half-hourly precipitation (GPM IMERG Final Precipitation L3, 0.1° × 0.1°) images were analyzed (Huffman et al., 2019). Although integrated multi-satellite retrievals for GPM (IMERG) algorithms have been improved to resolve diurnal cycles (Tan et al., 2019), there are still limitations in resolving small-scale features of rainfall events (Iyer and Drushka (2021b) and references herein). For this study, we chose the half-hour IMERG product, because it has high temporal resolution consistent with our observation time of less than 6 hr.

2.5. Statistical Tests

Salinity and temperature anomalies were categorized into different wind and solar radiation regimes, and statistical significance was determined using the Kruskal–Wallis test and the pairwise Wilcoxon test performed with R (version 4.2.1 [2022-06-23]) (see Tables S1 and S2 in Supporting Information S1). The results were considered significant when $p \leq 0.05$, with a 95% confidence level. The Chi^2 represents the sum of squared deviations for an expected pattern.

3. Results and Discussion

3.1. Effect of Wind and Solar Radiation on ΔS and ΔT

The two stations, 03 and 24, differed greatly in terms of anomalies, general trends, and small-scale features (see Figure 2). Generally, at station 03, ΔS was positive, and ΔT was negative. At station 24, an opposite trend was observed, with a negative ΔS and a positive ΔT. The mean ΔS values at stations 03 and 24 were 0.33 ± 0.72 and -0.13 ± 0.31 g kg^{-1}, respectively, and the mean ΔT values were -0.2 ± 0.18 and 0.19 ± 0.49°C, respectively. The combined ΔS and ΔT, that is, merged data from both stations (Figures 2b and 2c), differed significantly between three wind categories (ΔS: $p < 0.001$, $Chi^2 = 77.97$, ΔT: $p < 0.001$, $Chi^2 = 102.93$). At higher wind speeds (5.1–11.5 m s^{-1}), the anomalies from both stations approached zero (mean $\Delta S = -0.02 \pm 0.49$ g kg^{-1} and $\Delta T = -0.09 \pm 0.46$°C) due to the mixing processes (Figure 2b). At low wind speeds (0–2.0 m s^{-1}), evaporation drove ΔS to be positive ($\Delta S = 1.00 \pm 0.20$ g kg^{-1}) and ΔT to be negative ($\Delta T = -0.37 \pm 0.09$°C).

From lower to higher solar radiation, significant differences were observed from positive to negative ΔS (0.19 ± 0.57 to -0.23 ± 0.37 g kg^{-1}, $p < 0.001$, $Chi^2 = 63.26$) and from negative to positive ΔT (-0.14 ± 0.16 to 0.37 ± 0.59°C, $p < 0.001$, $Chi^2 = 191.68$), indicating that the SML is isolated from the underlying water masses and absorbs heat (Murray et al., 2000; Wurl et al., 2019). A pairwise Wilcoxon test showed that an increase in wind speed from low to high affects SSS ($p < 0.05$), but not an increase from low to medium wind speeds ($p > 0.05$). This is confirmed by the effect size, which shows only a medium-sized effect of wind speed on ΔS compared to the stronger effect size of wind on ΔT and solar radiation on ΔS and ΔT.

3.2. Response of ΔS and ΔT During Precipitation Events and Fronts

The results showed different responses of SSS and SST to precipitation, freshwater lenses, and fronts. Precipitation occurred at stations 03 and 24, but the temperature and salinity responses in the SML and bulk water were different and appeared to be closely related to the presence of salinity and temperature fronts (Figures 3–6) and to the near-surface meteorological variables (i.e., evaporation). At station 03 (Figure 3), the salinity at 1-m depth was consistently higher than that of the SML between 01:52 and 02:46 UTC (mean $\Delta S = -0.37 \pm 0.06$ g kg^{-1}), suggesting the presence of a shallow freshwater lens. After 02:46 UTC, S^3 appeared to enter a different water mass, while wind speed decreased from 5.8 m s^{-1} to 1.7 m s^{-1}. The salinity of the SML increased from 35.16 g kg^{-1} to 36.08 g kg^{-1}, and the temperature of the SML decreased from 28.70°C to 27.95°C. The salinity at 1-m depth showed the opposite trend and decreased from 35.65 g kg^{-1} to 34.89 g kg^{-1}, but the temperature decreased slightly from 28.70°C to 28.63°C (i.e., in the same direction but less compared to the SML). The mean anomalies of ΔS and ΔT (between 03:00 and 03:50 UTC) were 1.09 ± 0.07 g kg^{-1} and -0.31 ± 0.08°C, respectively, suggesting that the SML—and probably the near-surface layer shallower than 1 m — could have been an isolated water mass. Figure 3 confirms that the S^3 passed through two vertically separated water masses with a distinct stratification at station 03. The stratification seemed to persist, even though the density of the SML was higher than the density of the bulk water at 1-m depth between 02:40 and 03:50 UTC (Figure 3). Wurl et al. (2019) made similar observations with denser SML atop less dense bulk water, up to a maximum density difference of

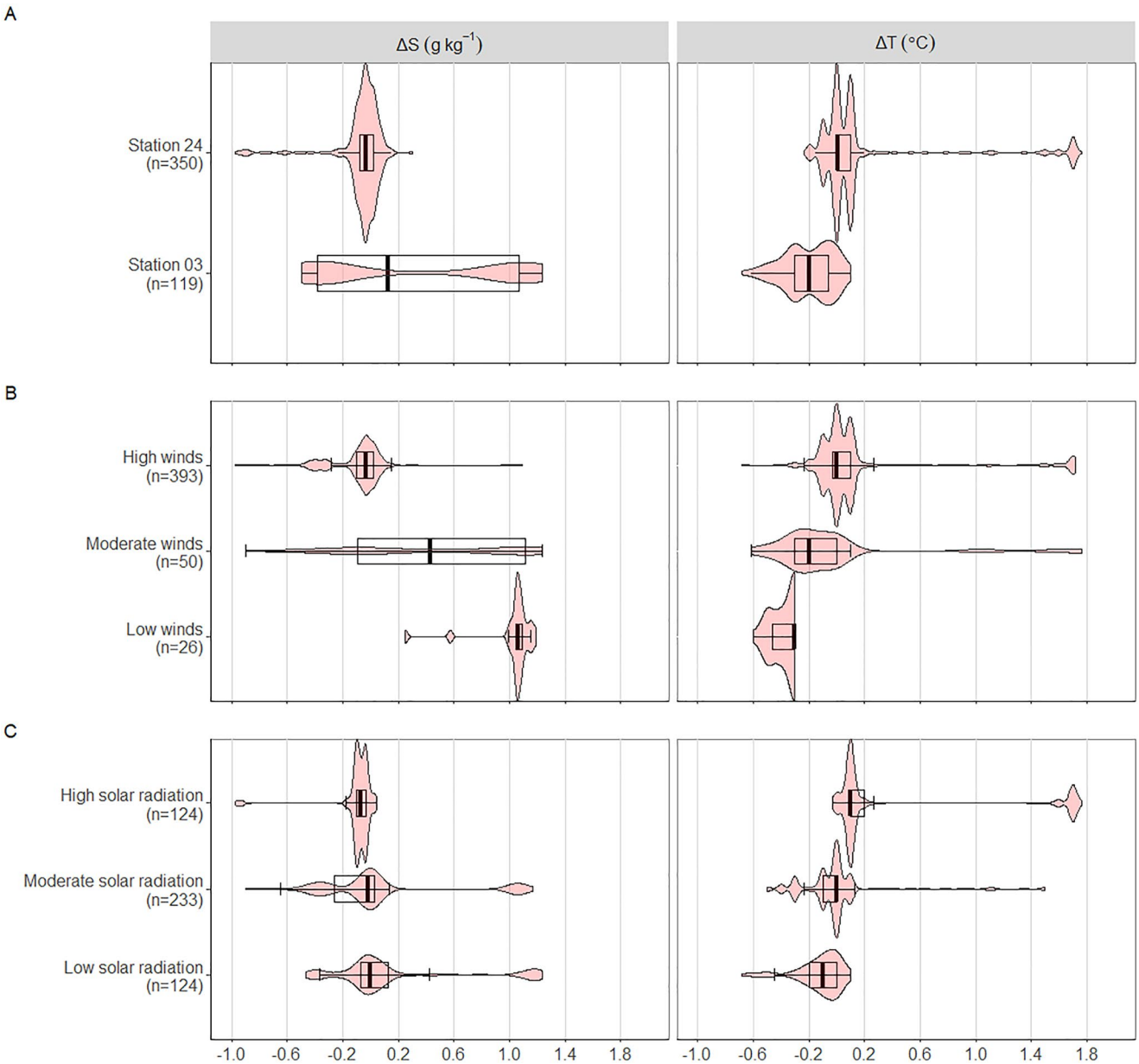

Figure 2. The violin plots (pink color) illustrate the data distribution and are based on a Gaussian kernel density estimation, including a whisker box plot of ΔS and ΔT (SML–bulk). (a) Stations 03 and 24, (b) three wind speed categories (low winds: 0–2 m s^{-1}, moderate winds: 2.1–5 m s^{-1}, and high winds: 5.1–11.6 m s^{-1}), and (c) solar radiation regimes (low solar radiation: <300 W m^{-2}, moderate solar radiation: 300–600 W m^{-2}, and high solar radiation: >600 W m^{-2}) of stations 03 and 24. Anomalies were calculated from the 1-min mean of SSS and SST. Error bars represent 5%–95% of the median values. Thick lines represent the median. *n* in parentheses is the number of observations.

1.3 g L^{-1}. In our case, we observed a maximum density anomaly of 1.0 g L^{-1}, confirming previous observations. Wurl et al. (2019) suggested that a denser SML could be held by interfacial tension, such as denser floating particles (Singh & Joseph, 2005). Zappa et al. (2009) pointed out that stratification (e.g., that induced by precipitation) causes near-surface turbulence to be trapped and vertical mixing to be reduced. Kudryavtsev and Soloviev (1990) showed that diurnal warming stabilizes near-surface layers (down to 2.5 m) in tropical oceans due to a decrease in wind-induced mixing. The combination of precipitation, diurnal warming, and reduced mixing could have caused a very shallow freshwater lens.

At station 24, between 19:42 and 20:07 UTC, we observed a decrease in salinity of 1 g kg^{-1} at 3-m depth, and 20 min later, a reduction of 0.5 g kg^{-1} in the SML and at 1-m depth (arrow a in Figure 3e). The optical

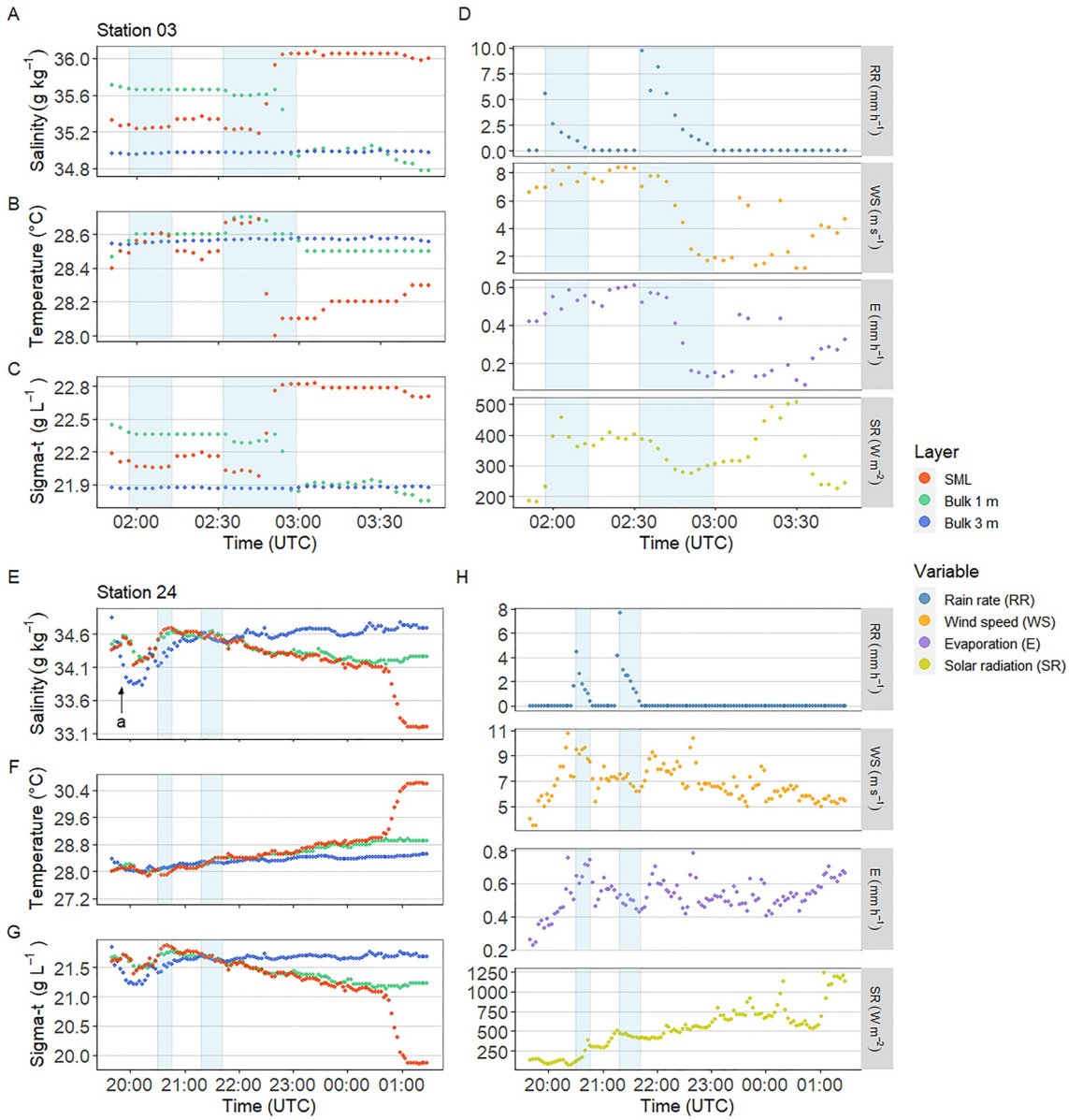

Figure 3. Time series of the 3-min mean from stations 03 and 24. (a and e) salinity, (b and f) temperature, and (c and g) sigma-*t* densities of three different ocean layers: sea surface microlayer (SML), bulk water from a 1-m depth (S^3), and bulk water from a 3-m depth (TSG); (d and h) rain rate (RR); wind speed (WS); evaporation (E); and solar radiation (SR).

rain sensor on the ship recorded a heavy rainfall event at a rate of up to 173.3 mm hr^{-1} (mean rain intensity = 23.24 ± 35.24 mm hr^{-1}) between 15:09 and 18:00 UTC before the deployment of S^3, suggesting that the water mass sampled between 19:42 and 20:07 was a freshwater lens generated 4 hr before by heavy rainfall. The 20-min offset in our observation was probably due to the spatial offset in the measurement from the RV Falkor (3-m depth) and S^3 (SML and 1-m depth). The distance between RV Falkor and S^3 ranged from 323 to 554 m during this time (see Figure S4 in Supporting Information S1). As the wind speed increased above 11 m s^{-1}, the freshwater lens was mixed with deeper water masses, as indicated by the nearly equal salinity in all three layers at around 20:20 UTC. Moulin et al. (2021) confirmed that freshwater lenses disperse at wind speeds greater than 10 m s^{-1}. However, Drushka et al. (2019) found that salinity and temperature anomalies (calculated from 1.1 minus 0.05 m) remained unaffected at wind speeds above 7 m s^{-1}. Riser et al. (2015) found comparable changes to our observations of salinity changes of 0.9 g kg^{-1} at 1-m depth 2 hr after the end of a rainstorm. At station 24, between 00:45 and 01:07 UTC, we observed extreme salinity and temperature gradients of −0.91 g kg^{-1}

and 1.50°C, respectively. Therefore, we suggest the existence of another, but very shallow, freshwater lens. A freshwater lens can persist for hours or days under lower wind speed conditions (Drushka et al., 2019; Iyer & Drushka, 2021a; Price, 1979; Reverdin et al., 2012, 2021; Thompson et al., 2019). Moulin et al. (2021) reported that most of the 28 freshwater lenses were observed at wind speeds of less than 5 m s^{-1}. Some of these freshwater lenses were warmer relative to ambient conditions due to heat absorption. From 00:45 onwards, the wind speed remained nearly constant at about 5 m s^{-1}, and the solar radiation increased, explaining the rising temperature in the SML. Figure 3g shows the density anomalies and confirms the presence of a less dense water mass on the sea surface (i.e., less saline and warmer freshwater lens in the SML). Soloviev and Lukas (1997) reported that the absorption of solar radiation enhances positive buoyancy and reduces the extent of turbulent mixing near the surface. Sharp fronts formed by precipitation and diurnal warming near the surface have been observed previously (Soloviev et al., 2002), and our measurements include the SML for the first time. Depending on the conditions at the air-sea boundary layer, these measurements confirm the existence of shallower freshwater lenses (<1 m deep), which would not have been detected with near-surface measurements at 1 m or below (Figure 3). The shallow freshwater lenses could be part of the evolution of deeper lenses with ongoing advection or formed by less freshwater input.

Both stations are in proximity to salinity and temperature fronts, which explains the large gradients in our data that occurred independent of rain events (Figure 6). Moreover, both stations are located within the South Pacific, with distinct freshwater pools (i.e., freshwater flux is dominated by precipitation) (Schanze et al., 2010), and were surrounded by major rainfall areas during the investigation periods (Figures 4 and 5). In addition, this region is characterized by low wind conditions through strong atmospheric convection (Hénin et al., 2019; Webster & Lukas, 1992). These large-scale processes, in combination with small-scale processes, such as local rainfall events, cause very high variabilities in SSS and SST, as reflected in our data.

3.3. Small-Scale Changes During Precipitation

We divided the rain events into Sta03-1, Sta03-2, Sta24-1, and Sta24-2 to discuss each event and the prevailing meteorological conditions driving the changes in SSS and SST (Figure 7). A summary of the results can be found in Table 1.

Sta03-1 (Figure 7a): At higher wind speeds (U_{10} = 7.60 ± 0.94 m s^{-1}) and light rain, the evaporation process (E = 0.61 ± 0.08 mm hr^{-1}) and the mixing of saltier water masses of deeper layers mask the effect of freshwater input from precipitation (RR = 2.37 ± 1.83 mm hr^{-1}). This is in line with the wind threshold of 7 m s^{-1}, at which no surface anomalies are observed (Drushka et al., 2019). The SSS in the SML oscillated at a frequency of 4 min, and with increasing salinity, the temperature decreased in parallel and vice versa. This oscillation pattern was also observed in density and confirmed similar observations in Wurl et al. (2019). At the beginning of the rain event (RR = 7.6 mm hr^{-1}), ΔS was −0.38 g kg^{-1}, but this was compensated by mixing and evaporation processes, as the RR dropped to below 2.5 mm hr^{-1}. However, freshwater input was sufficient to increase the temperature of the fresher SML by 0.17°C throughout the rain event. The increase in salinity by 0.17 g kg^{-1} and cooling by 0.18°C after the rain can even be attributed to evaporation, as the wind conditions remained similar. These moderate conditions of wind speeds and rain rate did not affect the salinity and temperature in the 1 and 3 m bulk water.

Sta03-2 (Figure 7b): At 02:41 UTC, the rain rate was the highest at 10.2 mm hr^{-1}, and the wind decreased slightly to 7 m s^{-1}. At this time, the salinity of the SML decreased by 0.06 g kg^{-1}, from ΔS = −0.32 g kg^{-1} before the rain to ΔS = −0.38 g kg^{-1} during precipitation. The temperature of the SML increased, suggesting that the rain temperature exceeded the SST. Toward the end of the rain event, our observations revealed sharp salinity and temperature gradients of 0.92 g kg^{-1} and −0.75°C, respectively, within 5–8 min in the SML, and −0.76 g kg^{-1} and −0.10°C, respectively, within 3–5 min at a depth of 1 m. ΔS turned from negative to positive (ΔS from −0.47 to 1.17 g kg^{-1}) and ΔT to a negative value (ΔT from 0.05 to −0.68°C), which is most likely attributable to a front, not to the observed rain event (Figure 4). The observations indicate that it was a near-surface phenomenon, as salinity and temperature were not affected at 3-m depth.

Sta24-1 (Figure 7c): At wind speeds of around 8 m s^{-1}, that is, in the higher range of our observations, the rainwater input of 2.31 ± 1.39 mm hr^{-1} was mixed very rapidly with more saline and colder bulk water. Rigorous mixing was supported by an increase in salinity at 3-m depth. A decrease in temperature (0.06°C min^{-1}) and an increase in salinity (0.05 g kg min^{-1}) in the SML between 20:29 and 20:35 UTC were observed as the wind

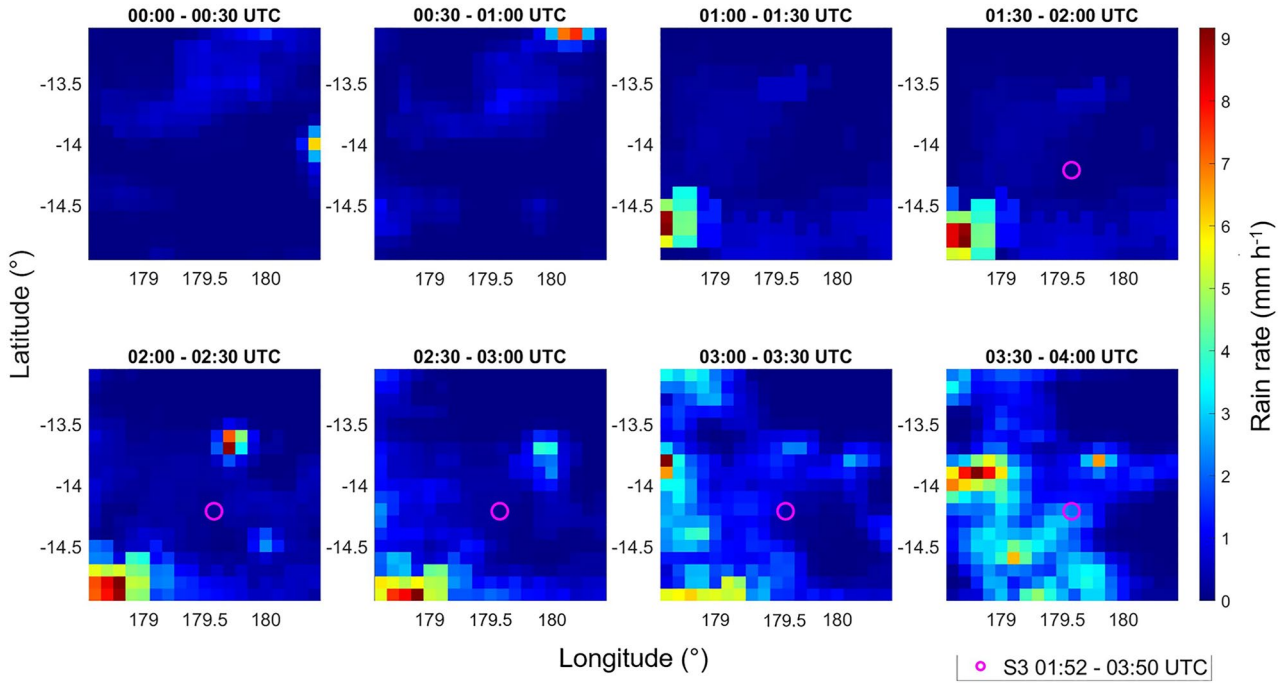

Figure 4. Half-hourly rain rate at station 03. The circle marks the position of S^3 during deployment. The color bar represents the rain rate.

speed increased from 7.5 m s^{-1} to 9.3 m s^{-1}. The effects on SSS in the SML were likely further enhanced by evaporative processes, as a cooling of SST was observed in the SML (mean $E = 0.62 \pm 0.07$ mm hr^{-1}, mean RR $= 3.95 \pm 1.02$ mm hr^{-1}). The temperature in the bulk water slightly increased during the rain period, at rates of 0.006°C min^{-1} and 0.015°C min^{-1} at 1-m and 3-m depths, respectively. Salinity also increased slightly in an oscillatory pattern (bulk 1 m = 0.01 g kg min^{-1} and bulk 3 m = 0.02 g kg min^{-1}).

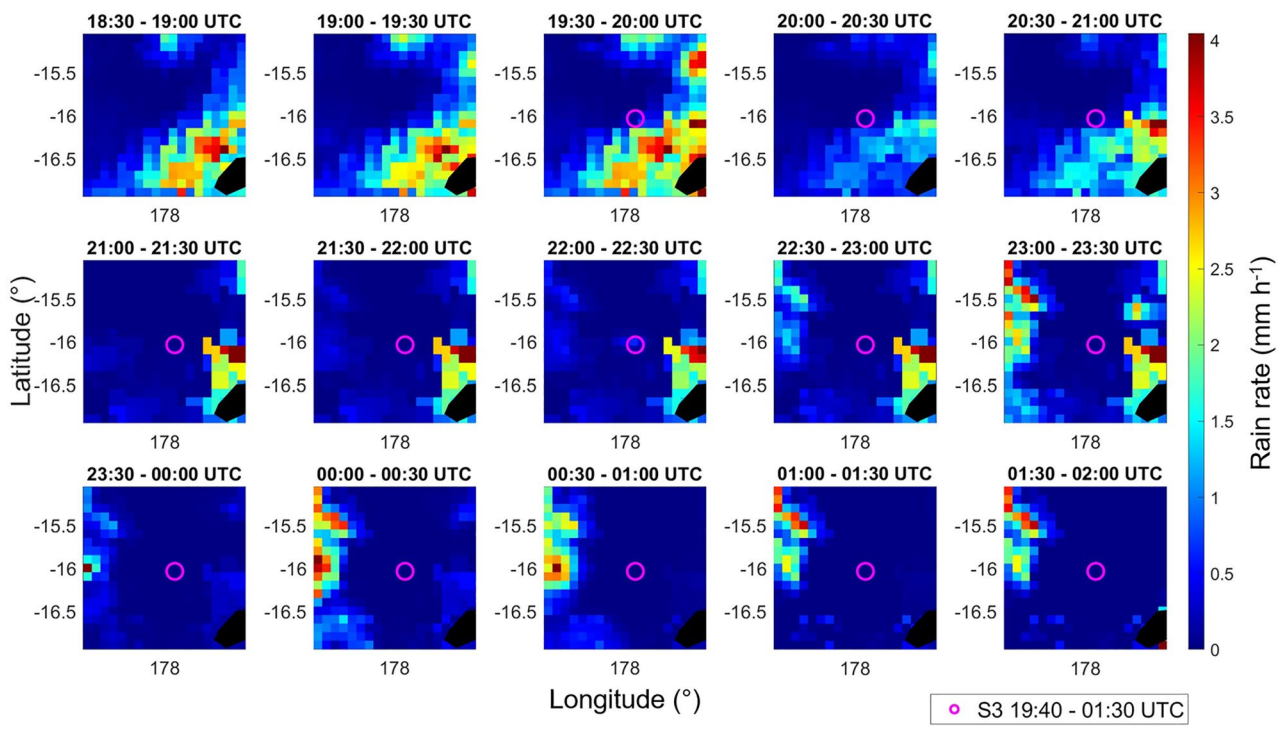

Figure 5. Half-hourly rain rate at station 24. The circle marks the position of S^3 during deployment. The color bar represents the rain rate.

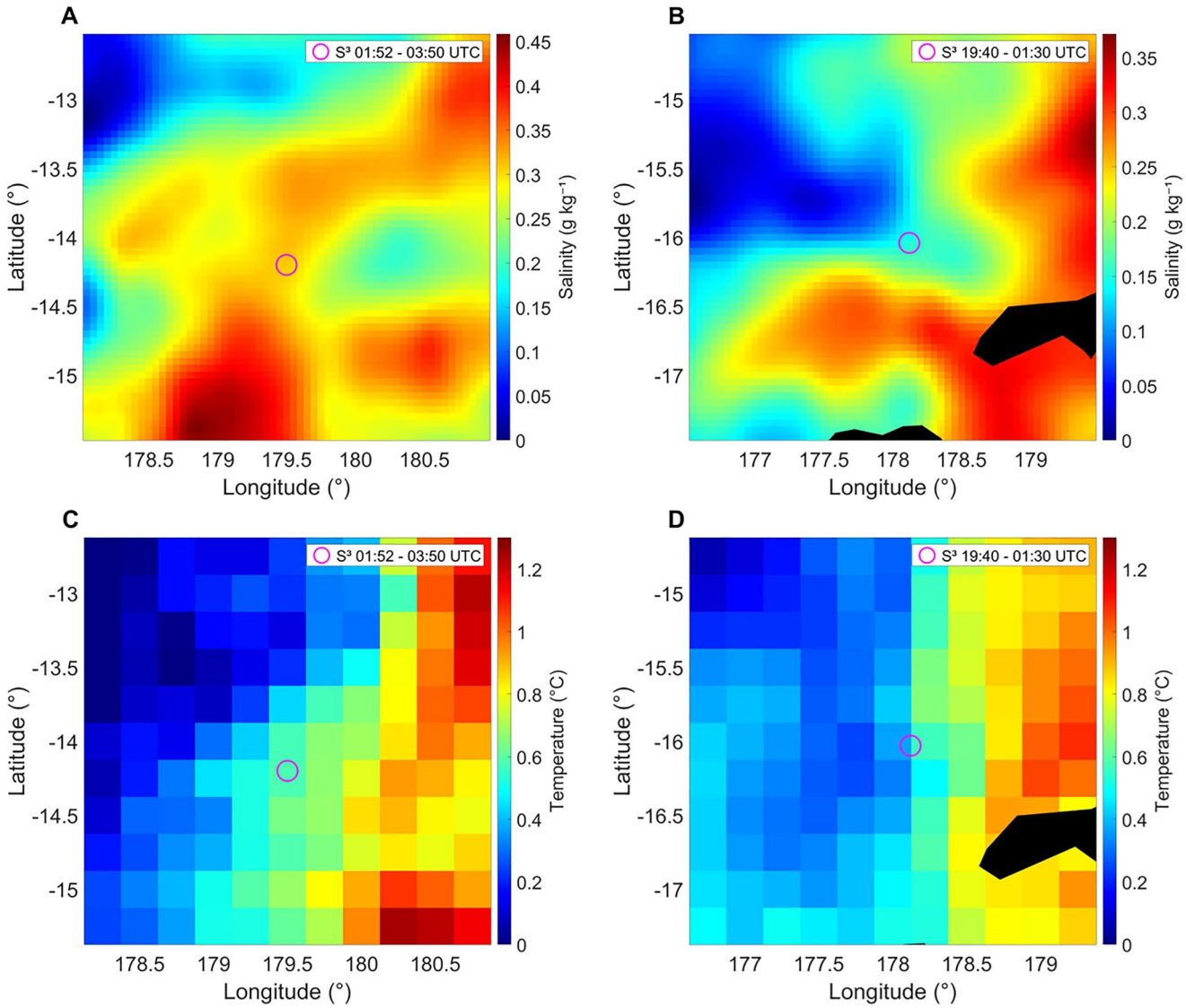

Figure 6. Satellite images of the mean SSS of the daily global Soil Moisture and Ocean Salinity (SMOS) (L4) product (a and b) and skin SST of the hourly product of the global ocean OSTIA diurnal skin sea surface temperature (c and d) of stations 03 (a and c) and 24 (b and d). The SST and SSS values are the difference to the lowest value (SSS/SST-lowest SSS/SST) within the shown map section. The circle marks the position of S^3.

Sta24-2 (Figure 7d): The wind speed was constantly above 7 m s^{-1} with no anomalies (i.e., mean $\Delta S = 0 \pm 0.04$ g kg^{-1} and $\Delta T = 0 \pm 0.04$°C). At 21:29 UTC, the wind decreased to 5.8 m s^{-1}, inducing anomalies (i.e., mean $\Delta S = -0.03 \pm 0.04$ g kg^{-1} and $\Delta T = -0.01 \pm 0.02$°C. The salinity in the SML and at 1-m depth water oscillated patterns without an up- or downward trend. This could indicate that the effects on salinity by precipitation, evaporation, and mixing were in equilibrium with small-scale temporal fluctuations. Salinity at 3-m depth decreased at 0.01 g kg^{-1} min^{-1}, indicating mixing with a slightly fresher water mass. The mixing occurred probably due to vertical entrainment from below and advection, as a similar trend could not be observed at 1-m depth in the SML. The data showed a temperature increase of 0.04°C min^{-1} in the SML and 0.002°C min^{-1} at 1-m depth between 21:21 and 21:34 UTC, indicating that the temperature of rain exceeded that of the surface, warming the upper water masses even at moderate wind speeds (i.e., exceeding evaporative cooling).

Wurl et al. (2019) performed complementary measurements using the S^3 and showed that salinity anomalies were driven not only by rain intensity but also by mixing processes at moderate and higher wind speeds. They demonstrated that lower rain intensities of less than 4 mm hr^{-1} could cause a ΔS decrease of 0.25 g kg^{-1} in the SML, without any change in the bulk water. It is intuitive to assume that the salinity of the SML depends strongly on the

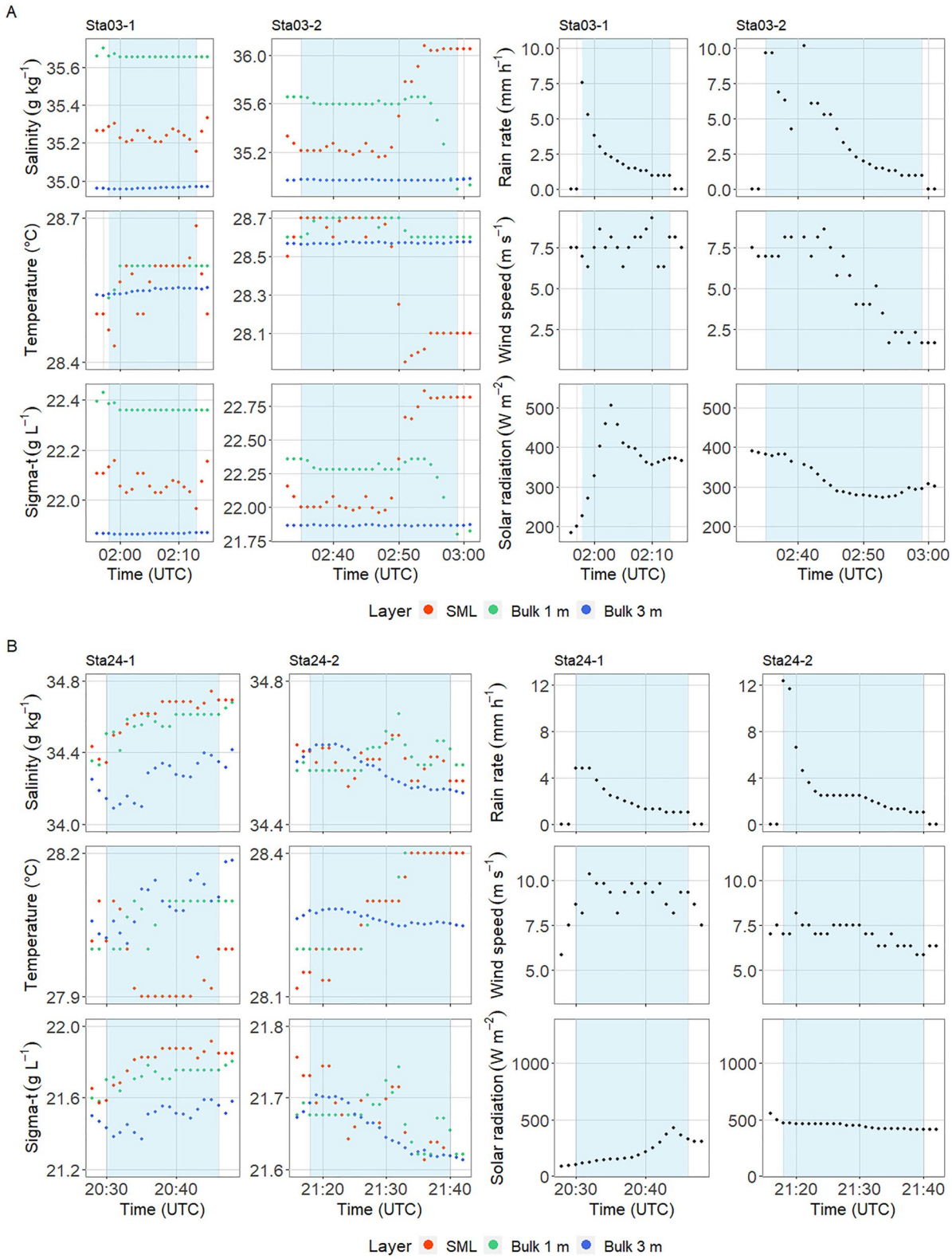

Figure 7. Zoomed in time series of the 1-min mean of salinity, temperature, density, rain rate, wind speed, and solar radiation during four rain events at stations 03 and 24. (a) Station 03, first rain event (Sta03-1) and second rain event (Sta03-2). (b) station 24, first rain event (Sta24-1) and second rain event (Sta24-2). There are three ocean layers: sea surface microlayer (SML), bulk water from a 1-m depth (S^3), and bulk water from a 3-m depth (TSG). The rain period is indicated as the light blue background.

Table 1
Summary of Small-Scale Changes in the Three Different Ocean Layers at All Stations and During All Rain Events

Station-rain event	SML	1 m	3 m	Mean RR (mm h^{-1})	Mean WS (m s^{-1})	Mean SR (W m^{-2})	Mean E (mm h^{-1})
Sta03-1	✓	✗	✗	2.37	7.60	378.78	0.61
Sta03-2	✓	✓	✗	4.00	5.26	315.47	0.44
Sta24-1	✓	✓	✓	2.31	9.25	216.36	0.66
Sta24-2	✓	✓	✓	3.20	6.95	441.91	0.49

Note. ✓ indicates that salinity and/or temperature showed changes during the rainfall. A ✗ indicates that salinity and temperature were not affected. Also shown are the mean rain rate (RR), wind speed (WS), evaporation (E), and solar radiation (SR) for each rain event.

rain rate. Nevertheless, in this study, we confirm that mixing processes and evaporation are essential counterparts in the observed freshening of the SML. This remains true for the lower rain intensities in this study compared to Wurl et al. (2019). In addition, the duration of rainfall and the accumulation of freshwater have been shown to play an important role (Asher et al., 2014; Drushka et al., 2019), but our observations include only short rain events. Laxague and Zappa (2020) found that longer gravity waves could be suppressed by heavy rain, which could increase surface roughness from droplet-generated ring waves. The average rain intensity during our measurements was not higher than 4 mm hr^{-1}; accordingly, the effect of the raindrops on the sea surface was rather small. Asher et al. (2014) hypothesized that SSS at a precipitation rate of less than 6 mm hr^{-1} is controlled by wind-induced mixing rather than the effect of freshwater. The lifespan and presence of freshwater lenses depend mainly on wind speed (Drushka et al., 2016, 2019; Moulin et al., 2021; Schanze et al., 2019) and do not exist with wind speeds higher than 7 m s^{-1} (Volkov et al., 2019). Over 80% of our measurements at stations 03 and 24 came from higher winds (5.1–11.6 m s^{-1}), leading us to conclude that the water masses were very well mixed. Our results further confirm that the SML responds almost instantaneously to the influence on evaporation and precipitation, and thus can play an important role in quantifying freshwater fluxes between the ocean and atmosphere.

4. Conclusions

This study presented comprehensive insights into how ΔS and ΔT respond to wind, evaporation, and solar radiation during rainfall events on a small scale, despite being limited to only two stations with rainfall events. The results confirmed that the SML could act as a proxy for wind-driven mixing and evaporation processes during light-to-moderate rainfall and that smaller amounts of freshwater mixed rapidly with the surrounding water masses. In regions with abundant precipitation, ΔS and ΔT were highly variable in time and space due to the formation of freshwater lenses with ΔS and ΔT of up to −1.11 g kg^{-1} and 1.77°C, respectively. The dynamic changes in these anomalies serve as a proxy for the fate of freshwater as evaporation and precipitation hit the upper sea surface first. Future studies in this area must take place on larger and longer scales to complete the understanding of ocean–atmosphere interaction processes on the sea surface. It must also be considered that precipitation properties such as droplet sizes and velocities play an important role in the formation of salinity and temperature anomalies at the SML. Measurements using an autonomous catamaran with a full range of rain intensities and characteristics could provide a comprehensive data set and clear insights.

Data Availability Statement

All data from the remotely operated catamaran from cruise FK191120 are with fully open access (Ribas-Ribas et al., 2022). In addition, we used the ship-based Shipboard Automated Meteorological and Oceanographic System data set for solar radiation (Smith et al., 2019) and the ship thermosalinograph data (https://doi.org/10.7284/908805, website: https://www.rvdata.us/search/cruise/FK191120). The L4 SMOS products are accessible via the website of the Barcelona Expert Center (https://bec.icm.csic.es/) and L2 data via the ESA website (https://smos-diss.eo.esa.int). We used the hourly product of the global ocean OSTIA diurnal skin sea surface temperature (https://doi.org/10.48670/moi-00165). Half-hourly precipitation (GPM IMERG Final Precipitation L3, 0.1° × 0.1°) images are available via the NASA's Earth Science Data Systems (https://disc.gsfc.nasa.gov/datasets/GPM_3IMERGHH_06/summary).

Acknowledgments
This work was funded by the German Research Foundation (DFG)—project numbers 427614800 and 451574234. We thank the RV Falkor crew and staff of the Schmidt Ocean Institute for providing ship time. We are grateful for the assistance of L. ter Hell during the expedition. We acknowledge C. Zappa and C. Witte for helpful discussions. L. Gassen thanks M. Schlundt from GEOMAR Kiel for providing a salinometer and we thank R. Herbst for her work on the evaporation calculation. Open Access funding enabled and organized by Projekt DEAL.

References

Asher, W. E., Jessup, A. T., Branch, R., & Clark, D. (2014). Observations of rain-induced near-surface salinity anomalies. *Journal of Geophysical Research: Oceans*, *119*(8), 5483–5500. https://doi.org/10.1002/2014jc009954

Donlon, C., Robinson, I., Casey, K., Vazquez-Cuervo, J., Armstrong, E., Arino, O., et al. (2007). The global ocean data assimilation experiment high-resolution sea surface temperature pilot project. *Bulletin of the American Meteorological Society*, *88*(8), 1197–1214. https://doi.org/10.1175/bams-88-8-1197

Drushka, K., Asher, W. E., Jessup, A. T., Thompson, E. J., Iyer, S., & Clark, D. (2019). Capturing fresh layers with the surface salinity profiler. *Oceanography*, *32*(2), 76–85. https://doi.org/10.5670/oceanog.2019.215

Drushka, K., Asher, W. E., Ward, B., & Walesby, K. (2016). Understanding the formation and evolution of rain-formed fresh lenses at the ocean surface. *Journal of Geophysical Research: Oceans*, *121*(4), 2673–2689. https://doi.org/10.1002/2015jc011527

Durack, P. J. (2015). Ocean salinity and the global water cycle. *Oceanography*, *28*(1), 20–31. https://doi.org/10.5670/oceanog.2015.03

Fairall, C. W., Bradley, E. F., Rogers, D. P., Edson, J. B., & Young, G. S. (1996). Bulk parameterization of air-sea fluxes for tropical ocean-global atmosphere coupled-ocean atmosphere response experiment. *Journal of Geophysical Research*, *101*(C2), 3747–3764. https://doi.org/10.1029/95jc03205

Gill, A. E., & Adrian, E. (1982). *Atmosphere-ocean dynamics* (Vol. 30). Academic Press.

Hénin, R., Ramos, A. M., Schemm, S., Gouveia, C. M., & Liberato, M. L. (2019). Assigning precipitation to mid-latitudes fronts on sub-daily scales in the North Atlantic and European sector: Climatology and trends. *International Journal of Climatology*, *39*(1), 317–330. https://doi.org/10.1002/joc.5808

Henocq, C., Boutin, J., Reverdin, G., Petitcolin, F., Arnault, S., & Lattes, P. (2010). Vertical variability of near-surface salinity in the tropics: Consequences for L-band radiometer calibration and validation. *Journal of Atmospheric and Oceanic Technology*, *27*(1), 192–209. https://doi.org/10.1175/2009jtecho670.1

Holthuijsen, L., & Herbers, T. (1986). Statistics of breaking waves observed as whitecaps in the open sea. *Journal of Physical Oceanography*, *16*(2), 290–297. https://doi.org/10.1175/1520-0485(1986)016⟨0290:sobwoa⟩2.0.co;2

Huffman, G., Stocker, E., Bolvin, D., Nelkin, E., & Tan, J. (2019). In A. Savtchenko (Ed.), *GPM IMERG Final Precipitation L3 1 day 0.1 degree × 0.1 degree V06*. Goddard Earth Sciences Data and Information Services Center (GES DISC). https://doi.org/10.5067/GPM/IMERGDF/DAY/06

Iyer, S., & Drushka, K. (2021a). The influence of preexisting stratification and tropical rain modes on the mixed layer salinity response to rainfall. *Journal of Geophysical Research: Oceans*, *126*(10), e2021JC017574. https://doi.org/10.1029/2021jc017574

Iyer, S., & Drushka, K. (2021b). Turbulence within rain-formed fresh lenses during the SPURS-2 experiment. *Journal of Physical Oceanography*, *51*(5), 1705–1721. https://doi.org/10.1175/jpo-d-20-0303.1

Katsaros, K. B. (1980). The aqueous thermal boundary layer. *Boundary-Layer Meteorology*, *18*(1), 107–127. https://doi.org/10.1007/bf00117914

Katsaros, K. B., & Buettner, K. J. (1969). Influence of rainfall on temperature and salinity of the ocean surface. *Journal of Applied Meteorology*, *8*(1), 15–18. https://doi.org/10.1175/1520-0450(1969)008⟨0015:iorota⟩2.0.co;2

Kleemann, M., & Meliß, M. (1993). Nutzungsmöglichkeiten regenerativer Energiequellen. In *Regenerative Energiequellen* (pp. 1–24). Springer. https://doi.org/10.1007/978-3-642-88075-9_1

Kudryavtsev, V. N., & Soloviev, A. V. (1990). Slippery near-surface layer of the ocean arising due to daytime solar heating. *Journal of Physical Oceanography*, *20*(5), 617–628. https://doi.org/10.1175/1520-0485(1990)020⟨0617:snslot⟩2.0.co;2

Laxague, N. J., & Zappa, C. J. (2020). The impact of rain on ocean surface waves and currents. *Geophysical Research Letters*, *47*(7), e2020GL087287. https://doi.org/10.1029/2020gl087287

Lindstrom, E., Bryan, F., & Schmitt, R. (2015). SPURS: Salinity processes in the upper-ocean regional study: The North Atlantic experiment. *Oceanography*, *28*(1), 14–19. https://doi.org/10.5670/oceanog.2015.01

Menon, S., Denman, K. L., Brasseur, G., Chidthaisong, A., Ciais, P., Cox, P. M., et al. (2007). *Couplings between changes in the climate system and biogeochemistry* (Technical Report). Lawrence Berkeley National Laboratory (LBNL).

Moulin, A. J., Moum, J. N., Shroyer, E. L., & Hoecker-Martínez, M. (2021). Freshwater lens fronts propagating as buoyant gravity currents in the equatorial Indian ocean. *Journal of Geophysical Research: Oceans*, *126*(8), e2021JC017186. https://doi.org/10.1029/2021jc017186

Murray, M., Allen, M., Merchant, C., Harris, A., & Donlon, C. (2000). Direct observations of skin-bulk SST variability. *Geophysical Research Letters*, *27*(8), 1171–1174. https://doi.org/10.1029/1999gl011133

Olmedo, E., González-Haro, C., Hoareau, N., Umbert, M., González-Gambau, V., Martínez, J., et al. (2021). Nine years of SMOS sea surface salinity global maps at the Barcelona Expert Center. *Earth System Science Data*, *13*(2), 857–888. https://doi.org/10.5194/essd-13-857-2021

Price, J. F. (1979). Observations of a rain-formed mixed layer. *Journal of Physical Oceanography*, *9*(3), 643–649. https://doi.org/10.1175/1520-0485(1979)009⟨0643:ooarfm⟩2.0.co;2

Reverdin, G., Morisset, S., Boutin, J., & Martin, N. (2012). Rain-induced variability of near sea-surface T and S from drifter data. *Journal of Geophysical Research*, *117*(C2), C02032. https://doi.org/10.1029/2011jc007549

Reverdin, G., Olivier, L., Foltz, G., Speich, S., Karstensen, J., Horstmann, J., et al. (2021). Formation and evolution of a freshwater plume in the northwestern tropical Atlantic in February 2020. *Journal of Geophysical Research: Oceans*, *126*(4), e2020JC016981. https://doi.org/10.1029/2020jc016981

Reverdin, G., Supply, A., Drushka, K., Thompson, E., Asher, W. E., & Lourenço, A. (2020). Intense and small freshwater pools from rainfall investigated during SPURS-2 on 9 November 2017 in the eastern tropical Pacific. *Journal of Geophysical Research: Oceans*, *125*(2), e2019JC015558. https://doi.org/10.1029/2019jc015558

Ribas-Ribas, M., Hamizah Mustaffa, N. I., Rahlff, J., Stolle, C., & Wurl, O. (2017). Sea surface scanner (S3): A catamaran for high-resolution measurements of biogeochemical properties of the sea surface microlayer. *Journal of Atmospheric and Oceanic Technology*, *34*(7), 1433–1448. https://doi.org/10.1175/jtech-d-17-0017.1

Ribas-Ribas, M., Stührenberg, J., Gassen, L., & Wurl, O. (2022). Multiparameter measurement of biogeochemical properties of the sea surface microlayer in the Pacific Ocean during R/V Falkor cruise FK191120 [Dataset]. PANGAEA. https://doi.org/10.1594/PANGAEA.940720

Riser, S. C., Anderson, J., Shcherbina, A., & D'Asaro, E. (2015). Variability in near-surface salinity from hours to decades in the eastern North Atlantic: The SPURS region. *Oceanography*, *28*(1), 66–77. https://doi.org/10.5670/oceanog.2015.11

Schanze, J., Schmitt, R. W., & Yu, L. (2010). The global oceanic freshwater cycle: A state-of-the-art quantification. *Journal of Marine Research*, *68*(3–4), 569–595. https://doi.org/10.1357/002224010794657164

Schanze, J., Springer, S., Thompson, E., Lagerloef, G., & Schmitt, R. (2019). Rain-induced freshwater lenses in the ITCZ – From observations to modeling. In *Geophysical Research Abstracts* (Vol. 21).

Shinki, M., Wendeberg, M., Vagle, S., Cullen, J. T., & Hore, D. K. (2012). Characterization of adsorbed microlayer thickness on an oceanic glass plate sampler. *Limnology and Oceanography: Methods*, *10*(10), 728–735. https://doi.org/10.4319/lom.2012.10.728

Singh, P., & Joseph, D. (2005). Fluid dynamics of floating particles. *Journal of Fluid Mechanics*, *530*, 31–80. https://doi.org/10.1017/s0022112005003575

Smith, S. R., Rolph, J. J., Briggs, K., & Bourassa, M. A. (2019). Quality controlled shipboard automated meteorological and oceanographic system (SAMOS) data [Dataset]. National Centers for Environmental Information. http://samos.coaps.fsu.edu

Soloviev, A., & Lukas, R. (1997). Observation of large diurnal warming events in the near-surface layer of the western equatorial Pacific warm pool. *Deep Sea Research Part I: Oceanographic Research Papers*, *44*(6), 1055–1076. https://doi.org/10.1016/s0967-0637(96)00124-0

Soloviev, A., Lukas, R., & Matsuura, H. (2002). Sharp frontal interfaces in the near-surface layer of the tropical ocean. *Journal of Marine Systems*, *37*(1–3), 47–68. https://doi.org/10.1016/s0924-7963(02)00195-1

Tan, J., Huffman, G. J., Bolvin, D. T., & Nelkin, E. J. (2019). Diurnal cycle of IMERG V06 precipitation. *Geophysical Research Letters*, *46*(22), 13584–13592. https://doi.org/10.1029/2019gl085395

Terray, L., Corre, L., Cravatte, S., Delcroix, T., Reverdin, G., & Ribes, A. (2012). Near-surface salinity as nature's rain gauge to detect human influence on the tropical water cycle. *Journal of Climate*, *25*(3), 958–977. https://doi.org/10.1175/jcli-d-10-05025.1

Thompson, E. J., Moum, J. N., Fairall, C. W., & Rutledge, S. A. (2019). Wind limits on rain layers and diurnal warm layers. *Journal of Geophysical Research: Oceans*, *124*(2), 897–924. https://doi.org/10.1029/2018jc014130

Volkov, D. L., Dong, S., Foltz, G. R., Goni, G., & Lumpkin, R. (2019). Observations of near-surface salinity and temperature structure with dual-sensor Lagrangian drifters during SPURS-2. *Oceanography*, *32*(2), 66–75. https://doi.org/10.5670/oceanog.2019.214

Webster, P. J., Clayson, C. A., & Curry, J. A. (1996). Clouds, radiation, and the diurnal cycle of sea surface temperature in the tropical western Pacific. *Journal of Climate*, *9*(8), 1712–1730. https://doi.org/10.1175/1520-0442(1996)009⟨1712:cratdc⟩2.0.co;2

Webster, P. J., & Lukas, R. (1992). TOGA COARE: The coupled ocean–atmosphere response experiment. *Bulletin of the American Meteorological Society*, *73*(9), 1377–1416. https://doi.org/10.1175/1520-0477(1992)073⟨1377:tctcor⟩2.0.co;2

Willett, K. M., Gillett, N. P., Jones, P. D., & Thorne, P. W. (2007). Attribution of observed surface humidity changes to human influence. *Nature*, *449*(7163), 710–712. https://doi.org/10.1038/nature06207

Wurl, O., Landing, W. M., Mustaffa, N. I. H., Ribas-Ribas, M., Witte, C. R., & Zappa, C. J. (2019). The ocean's skin layer in the tropics. *Journal of Geophysical Research: Oceans*, *124*(1), 59–74. https://doi.org/10.1029/2018jc014021

Zappa, C. J., Ho, D. T., McGillis, W. R., Banner, M. L., Dacey, J. W., Bliven, L. F., et al. (2009). Rain-induced turbulence and air-sea gas transfer. *Journal of Geophysical Research*, *114*(C7), C07009. https://doi.org/10.1029/2008jc005008